



Mechanical and interfacial analysis of 3D-printed two-matrix continuous carbon fibre composites for enhanced structural performance



Fei Liu^a, Shenru Wang^a, Wuxiang Zhang^{a,*}, Xilun Ding^a, Eleonora Ferraris^b, Jan Ivens^{b,c,*}

^a School of Mechanical Engineering and Automation, Beihang University, Beijing, China

^b KU Leuven, Technology Campus De Nayer, Sint-Katelijne-Waver, Belgium

^c KU Leuven, Dept. of Materials Engineering, Sint-Katelijne-Waver, Belgium

ARTICLE INFO

Keywords:

- A. Carbon fibres
- E. 3-D printing
- D. Microstructural analysis
- B. Fracture

ABSTRACT

Two-matrix continuous carbon fibre composites are recognized for enhancing structural and mechanical properties. However, a comprehensive investigation into their interfacial behaviour and potential has yet to be undertaken. Based on the 3D printing process, this study uses experimental and simulation techniques to analyse the mechanical and interfacial performance across multiple scales. The flexure properties under different processing parameters are studied at the macro level. Meso and micro-structural characterization are evaluated by scanning electron microscopy, optical microscopy and molecular dynamics simulation. The disparities in simulations and experimental results are attributed to macroscopic defects and reinforcement volume fraction. This yields insights into strategies for optimising performance, culminating in a comprehensive understanding of the fracture mechanism of two-matrix continuous carbon fibre composites. Our study provides an approach to creating and analysing other systems with multiple matrix composites and enabling new engineering applications for composites.

1. Introduction

Fibre-reinforced polymer composites are renowned for their distinctive structural and mechanical properties, rendering them invaluable in a wide range of lightweight applications. These applications span various industries, including transportation (such as aerospace [1–3], automotive [4–6], railway [7,8]), medical (rehabilitation products [9–11], joint prosthesis [12–14]) and beyond [15–17]. Continuous carbon fibre-reinforced polymer composites, in particular, have garnered significant attention when compared to other reinforcement types. The majority of current continuous carbon fibre-reinforced polymer composites comprise oriented fibres within a polymeric matrix, resulting in a synergistic combination of strength and stiffness. However, these exceptional properties are often hindered by relatively low mechanical characteristics, especially in terms of adhesion bonding strength [18].

The strategies to enhance structural performance in continuous carbon fibre-reinforced polymer composites involve the introduction of two matrix for accommodating heterogeneous materials like

thermoplastic and thermoset matrices [19–22]. Thermoplastic matrices show excellent mechanical (especially toughness) and chemical performance, as well as easy processability [20,23,24], and thermosetting polymer matrices, are specifically suited for fibre-reinforced polymer composites due to their low viscosity and wettability of the carbon fibres. One of the first researches on two-matrix composites was glass fibre reinforced thermoset and thermoplastic composites to obtain a better transverse strain capacity, initially reported by Vasil'ev and Salov [19]. The results showed that tensile failure strain and the specific strength were improved to 3 % and 18 %, respectively. Further, a two-matrix composite comprising carbon fibres embedded in a stiff and flexible baseline epoxy matrix was manufactured by Callens and Bergsma [21]. They selected this two-matrix composite based on its unprecedented flexibility and strength. Then they verified that this type of composite could deliver a better compression strength and minimise interface defects. Still, more comprehensive investigations into the mechanics of two-matrix continuous carbon fibre composites are recommended to fully explore the failure mode and interfacial characteristics and tap the potential of the materials.

* Corresponding authors at: School of Mechanical Engineering and Automation, Beihang University, Beijing, China (W. Zhang). KU Leuven, Technology Campus De Nayer, Sint-Katelijne-Waver, Belgium (J. Ivens).

E-mail addresses: feiliulf@buaa.edu.cn (F. Liu), srwang@buaa.edu.cn (S. Wang), zhangwuxiang@buaa.edu.cn (W. Zhang), xlding@buaa.edu.cn (X. Ding), eleonora.ferraris@kuleuven.be (E. Ferraris), jan.ivens@kuleuven.be (J. Ivens).

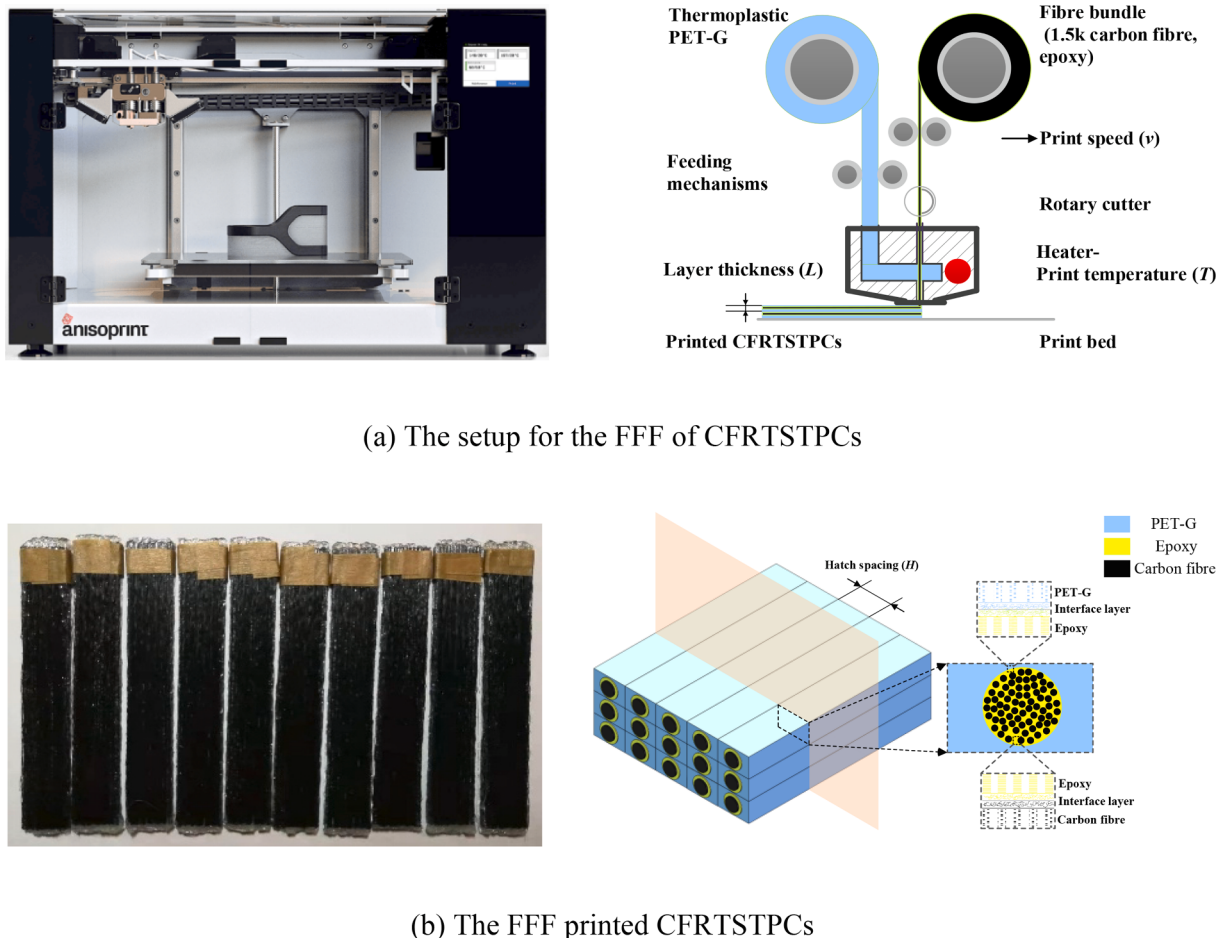


Fig. 1. The process principle and schematic of Anisoprint printing process for CFRTSTPCs.

Meanwhile, a wide variety of fabrication techniques have lately emerged along with the growth in the use of continuous fibre composites. Among them, fused filament fabrication (FFF) of composites is one of the most appealing processes to achieve satisfying mechanical properties, which feeds continuous filaments from spools through a heated nozzle and then the molten material is extruded onto the platform following a given route [25]. Unlike other techniques, this process is much more material-efficient and cost-saving for the combinations of two or more materials, fulfilling the particular interest of the production chain modification [26,27]. For example, Markforged Company developed an industrial additive manufacturing platform for continuous fibre fabrication based on a polyamide (PA) matrix [28]. Another FFF-based equipment was developed for polylactide (PLA) and 1 k carbon fibre tow that delivered a flexural strength of 335 MPa with a fibre volume content of 27 % [27]. Currently, based on a thermoset-thermoplastic matrix composite, Azarov and Adi et al. [20,22] presented a carbon fibre reinforced polymer (CFRP) printing technology for producing high-performance composite parts. Herein, the FFF is a sensitively reacting technique characterized by a considerable number of inputs of raw material and process parameters [29].

Process parameters investigation of FFF has been conducted for years to improve manufacturing quality. Using numerical simulation, Shahriar et al. [30] investigated the influence of nozzle diameter, feed rate and layer height on rheological behaviour in the liquefier. They further found that the shear rate increases with higher inlet velocities and smaller diameters, indicating the correlation between shear rate and surface defects. A full-factorial designed experiment was also used to analyse the influence of process parameters including build orientation, print speed and layer thickness, on tensile and compression strengths.

The significance of each process parameter on the properties was statistically investigated [31]. Multiple advanced algorithms have been utilized to optimise process parameters and then achieve substantial improvements in performance [32,33]: for example, using the naked mole-rat algorithm, Chohan et al. [33] selected maximum impact strength, flexural strength and tensile strength as the objectives and five different parameters as the augments in macro level. A major drawback of previous research is that experimental-based methodologies are hard to reveal the changes in atomic structure and molecular movements which will affect composite's macro properties. Specifically, the degree to which mechanical properties can be attained depends on the molecular state of reinforcement, polymer and interfacial bonding strength, which is affected by the designed manufacturing process and process parameters.

To circumvent such drawbacks and shift from morphological to molecular level, theoretical modelling and computational simulation have been gradually applied to study composites and could provide some crucial perspectives. For this reason, many researchers use the first principle methods [34–36], molecular dynamics method [37–40], and continuum mechanics theories [41–43] to reveal atom and molecular conformation of composite systems in the interfacial area of different constituting elements. For example, Galos et al. [34] used the first principle to estimate the electrical conductivity of 3D printed continuous carbon fibre composites in the longitudinal and transverse directions and showed that higher fibre waviness increased fibre contact through-thickness direction. A periodical supercell model of polymer epoxy/BMI composites was studied by Sachdeva [36] using density functional theory-based first principles, which can accurately and efficiently predict the response on the bonding strength and transverse

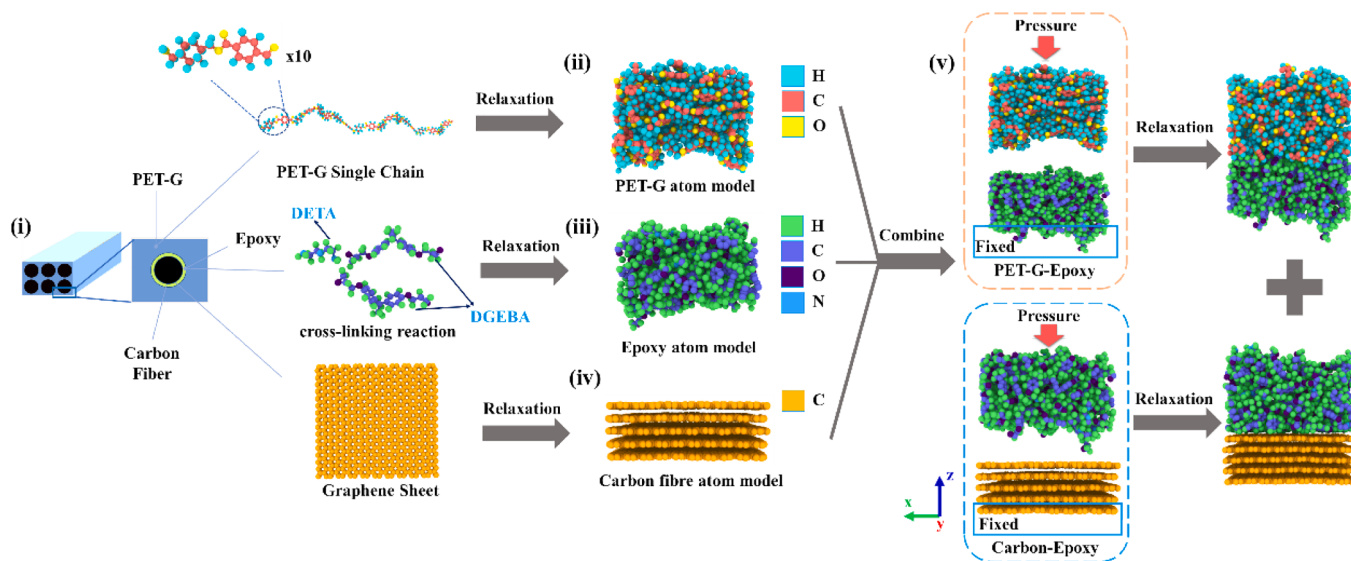


Fig. 2. Schematic diagram of the modelling process for all-atom models including PET-G, epoxy and carbon fibre in BIOVIA Materials Studio.

stiffness. Han and Elliott [37] calculated elastic moduli under different volume fractions of carbon nanotubes using the molecular dynamics method and attested that the interfacial interaction enhances the elastic properties when comparing the simulation results with the macroscopic rule-of-mixtures. Using a similar methodology, Yan et al. [38] analysed carbon fibre/polyimide composites grafted with different functional groups to figure out the relationship between the functional groups and interface mechanical properties. Continuum mechanics theories are normally used to investigate microscale or nanoscale structures, like Shokrieh and Rafiee [41] predicted Young's modulus of graphene sheets and carbon nanotubes. The previous results showed that multi-scale characteristics of interfacial behaviour and mechanical performance can be calculated and reflected by computational simulation. Despite this, the reinforcement mechanism of the two-matrix continuous carbon fibre composite interface still remains ambiguous and needs to be resolved, which is the focus of current research.

Hence the motivation of the paper is to analyse the influence of process parameters on two interface behaviours and mechanical characteristics of two-matrix continuous carbon fibre composites via a combination of experimental methodologies and computational investigations. Through 3-point bending tests, the flexural properties under different processing parameters are provided, and the bending failure modes are assessed by combining meso- and micro-structural characterisation. We further create a molecular dynamic model for the two-matrix-based composites. The interaction energy and elastic moduli with different boundary conditions and fibre volume fractions are obtained here. The molecular dynamic simulations allow direct comparison of the experimental results in multi-scales, thereby strengthening how to maximise the advantages of two-matrix composites in the manufacturing process. In this study, this approach provides an understanding of the interface behaviours during FFF and fracture patterns of two-matrix continuous carbon fibre composites.

2. Experimental method

2.1. Materials

Transparent polyethylene terephthalate glycol-modified (PET-G) filament is supplied by REC company, Moscow, Russia, and it is their thermoplastic blend of matrix (1.75 mm in diameter and 1.3 g/cm³ in density). Before processing, this polymer was stored in an oven at 120 °C for 12 h to protect the filament against deterioration due to moisture absorption. The reinforcing carbon fibre (TC-33) is supplied by Formosa

Corp. These are comprised of fibres bundles, impregnated with a special polymer (epoxy, thermoset matrix). Bundles of carbon fibres were 350 µm in diameter, each bundle constituting ~1500 fibres. Based on the previous thermogravimetric analysis [44], the volume fraction of carbon fibre in the impregnated bundles is 60 %. All information on mechanical properties and chemical composition of the fibres and matrix is provided by the mentioned supplier. These materials are prepared for the Anisoprint composer A3 printer.

2.2. Experiments design

Mechanical properties and interfacial behaviour of the printed samples were evaluated by means of flexural strength, modulus, topography analysis and fracture modes. In fact, both processing parameters (temperature, printing speed, layer thickness, hatch spacing, infill configuration) and material properties will influence these characteristics. Based on the parameter effects on the mechanical quality response seen in the previous study [44,45], decreasing the hatch spacing (H), layer thickness (L), and printing speed (V), while increasing the nozzle temperature (T), lead to enhanced mechanical properties as shown in Fig. 1. For this reason, the nozzle temperature was gradually decreased, until the lowest values available for the material printing process were reached; then, the printing speed and hatch spacing were gradually increased until the maximum values available on the printing machine were obtained. Since both layer thickness and hatching spacing will affect the volume fraction of carbon fibre, here the layer thickness here was held constant. The visualisation of the effect of processing parameters on flexural properties and interfacial behaviour could be given and investigated. A laminate of 10 mm × 80 mm × 2 mm was fabricated in 0° raster angle (longitudinal). According to ASTM standard [46], the support span L was 64 mm extracted from the span to thickness ration of 32:1. Finally, a universal testing equipment (Instron 5567) was employed and applied a fixed loading rate of 2 mm/min. Following stress-strain curves, the maximum flexural strength and the flexural modulus were obtained.

2.3. Meso and micro-structural characterization

To understand the interfacial behaviour of the two-matrix continuous carbon fibre composites under flexural loads, we characterised the FFF printed unidirectional CFRTSTPCs structures at meso- and micro-structural scales employing SEM, and optical microscopy. The local surface morphologies of CFRTSTPCs with different process parameters

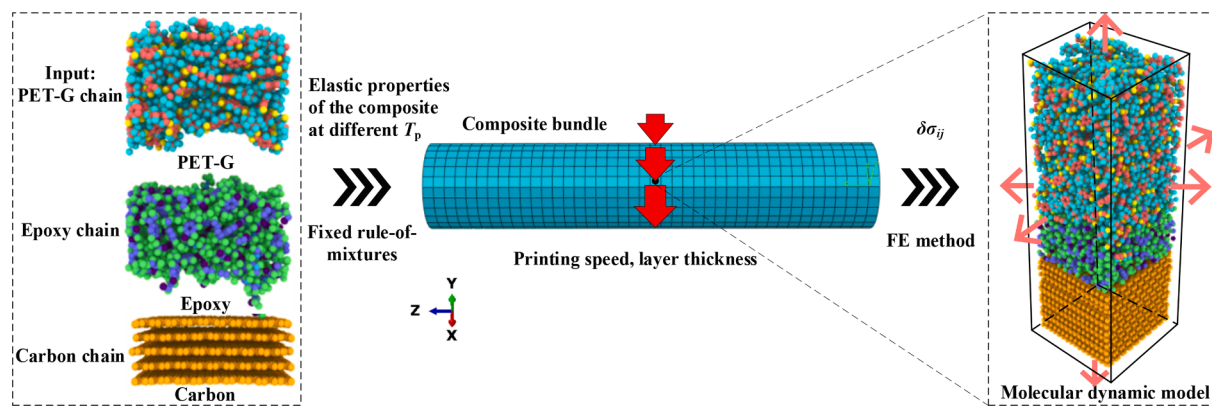


Fig. 3. Schematic diagram of current multiscale approach and boundary parameters transfer process in two interfacial interaction models.

Table 1
3D printing process parameters of CFRTSTPCs used in this work.

Tr.	Temperature (°C)	Printing speed (mm/min)	Hatch spacing (mm)	Other parameters	Fibre fraction (%)	Epoxy fraction (%)
1	245	150	0.55	layer thickness 0.36 mm, aligned configuration	29.1	19.4
2	230	150	0.55		29.1	19.4
3	215	150	0.55		29.1	19.4
4	200	150	0.55		29.1	19.4
5	200	300	0.55		29.1	19.4
6	200	600	0.55		29.1	19.4
7	200	600	0.75		21.3	14.2
8	200	600	0.95		16.8	11.2

Table 2
Elastic properties of PET-G.

Temperature (°C)	Elastic modulus (GPa)	Shear modulus (GPa)	Poisson's ratio
27	2.030	0.742	0.368
200	1.530	0.553	0.383
215	0.899	0.361	0.244
230	0.750	0.336	0.117
245	0.610	0.282	0.082

Table 3
Elastic constants of carbon fibre bundles.

E_1 (GPa)	E_2 (GPa)	G_{12} (GPa)	G_{23} (GPa)	ν
154	7.5	4.5	4.5	0.31

after bending failure were first observed by Tescan VEGA3 SEM. To improve the quality of SEM images, a vacuum plating method was first used to spray gold on the fracture surface. The fracture behaviour and the local interfacial performance of broken cross-sectional surfaces were evaluated by scanning electron microscopy. Meanwhile, the printed parts were transversely sectioned, polished and finished for microstructural analysis to observe the coating quality and void distribution. The presence of voids, and bulk imperfections such as bundle fracture, bundle deformation and distribution are thoroughly investigated depending on the particular print conditions. Such mesoscale analysis allowed the acquisition of void distribution in the final FFF printed

sample.

3. Numerical simulation methodology

The molecular dynamics method is a simulation method for analysing the physical movements of molecules that employs Newton's laws (classical mechanics), and can qualitatively offer a window into the microscopic dynamical behaviour between the individual components. In order to provide a dynamic evolution view at an atomic scale and analyse the interdiffusion of molecule chains across the heterogeneous interface, this section first depicts the two molecular dynamic models for the two-matrix continuous carbon fibre composite interface. From this information, the microscopic mechanisms of interfacial bonding energy and elastic properties can be calculated under different process parameters. Particularly, the atomistic model of CFRTSTPCs was built using Large-scale Atomic/Molecular Massively Parallel Simulation (LAMMPS) [47] and the atomic images were observed in OVITO [48].

3.1. Preparation of molecular structure

The simulation system was composed of carbon fibre, epoxy, and PET-G, as shown in Fig. 2(i). In general, the outer surface of carbon fibre is graphite plates parallel to the fibre surface even though these graphite plates are modified due to electrochemical treatment inducing oxygen groups. Since we assumed that the atomic structure is similar to graphene [49–51], the continuous carbon fibre surface is simplified as a multi-layer graphene model (Fig. 2(ii)) with a C-C bond length of 1.42 \AA and stacking distance of 3.4 \AA [52,53].

Table 4
Compaction stress applied in trials.

Tr.	Compaction stress (MPa)						
1	-0.00565	3	-0.01104	5	-0.01599	7	-0.97799
2	-0.00719	4	-0.02603	6	-0.00867	8	-0.9507

The atomistic interactions of carbon fibre were described by the adaptive intermolecular reactive empirical bond order potential (AIR-EBO) [54]. The epoxy model (Fig. 2(iii)) was constructed with the crosslink of Diglycidyl ether of bisphenol A (DGEBA) and Diethylenetriamine (DETA), and the ratio between them should maintain 2:1 [55]. The crosslink reaction of epoxy was simulated at 500 K (around 230 °C) [56] with a maximum reaction radius of 5 \AA for 1 ns. Then, the epoxy system was gradually cooled down to 300 K (around 27 °C) and following equilibrated at 27 °C for 1 ns to obtain a stable structure (fully cured). The amorphous PET-G model (Fig. 2(iv)) was constructed with a target density of 1.3 g/cm³ and each polymer chain of PET-G had 10 repeat units.

The CFRTPTS system was equilibrated and calculated with a canonical (NVT) ensemble. After obtaining the initial structure of the carbon fibre, cured epoxy resin, and PET-G models, all the initial structures were equilibrated with an NVT ensemble at 27 °C for 1 ns to release the residual stress and obtain the low-energy conformations. The time step adopted in the simulation was 1 fs. Though 3D printing is a dynamic process in which temperature changes affect molecular mobility, and hence the development of intimate contact at the PET-G and impregnated bundle interface, the initial printing temperature in the interface is used to simulate the processes. It is justified because complete intimate contact is assumed at the interface.

Polymer consistent force field (PCFF) was chosen to describe the atomistic interactions of PET-G and epoxy [57]. Based on previous research, PCFF was also applicable to the simulation of the interaction between carbon fibre and polymer [58,59]. The non-bonded interaction energy was described by the 9–6 Lennard-Jones (LJ) potential. The 9–6 LJ potential [60] is shown as Eq. (1):

$$E_{\text{interfacial}} = \varepsilon_{\text{potential}} \left[2 \left(\frac{r_{\text{atom}}}{r} \right)^9 - 3 \left(\frac{r_{\text{atom}}}{r} \right)^6 \right] r < r_c \quad (1)$$

where $E_{\text{interfacial}}$ is the interaction energy, $\varepsilon_{\text{potential}}$ is the depth of the potential well, r_{atom} represents the distance at zero interatomic interactions, r is the interatomic distance and r_c is the cutoff distance. The cutoff distance was 10 \AA, and the non-bonded interaction energy

between them would be neglected when the distance between two atoms was greater than 10 \AA.

To simulate the interface forming process during the actual printing process, the combination of the carbon fibre-epoxy system (or carbon-epoxy system) and PET-G-epoxy system were performed, respectively. During the simulation of the interface forming process, the carbon fibre and epoxy models were placed in a box with a size of 42.6 \AA × 39.3511 \AA × 50 \AA, and the carbon-epoxy system was equilibrated at different temperatures with a pressure at the top atoms of epoxy and a fix at the bottom of carbon fibre. Moreover, the same operations were applied to the PET-G-epoxy system with a box size of 42.6 \AA × 39.3511 \AA × 50 \AA but with a pressure at the top atoms of PET-G and a fix at the bottom of the epoxy. This PET-G model was composed of 10 chains. Furthermore, to realistically simulate the continuity of CFRTSTPCs, periodic boundary conditions (PBCs) were applied in the x and y directions.

3.2. Boundary conditions

The FFF printing process consists of two steps, each of which is carried out by a printing nozzle and a 3 DOF platform. These steps are firstly melting matrix and coating reinforcing filament in the printing nozzle, and secondly composites printing following pre-set route and layer thickness. In the second step, multiple interactions occur between the deposited material and the nozzle, which are affected by various processing parameters, such as printing speed, layer thickness, printing temperature, etc. In this situation, characterizing the boundary conditions of the deposited material at specific printing status helps to construct molecular models precisely and investigate these interfacial behaviours. For this reason, the printing process was then modelled and stimulated by the FEM (Finite Element Method), as illustrated in Fig. 3. The FEM model includes a printing nozzle and a single composite bundle, in which a dynamic stress analysis was carried out in ABAQUS. The printing speed along the pre-set route, printing layer thickness and other external conditions are applied to precisely display the dynamic behaviour of the deposited material caused by the printing process.

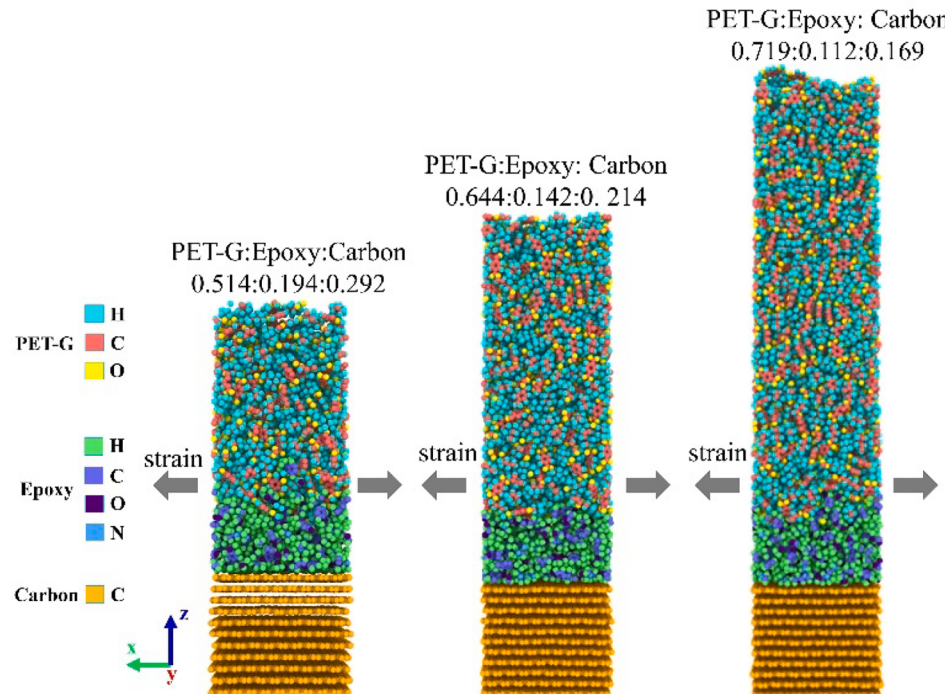
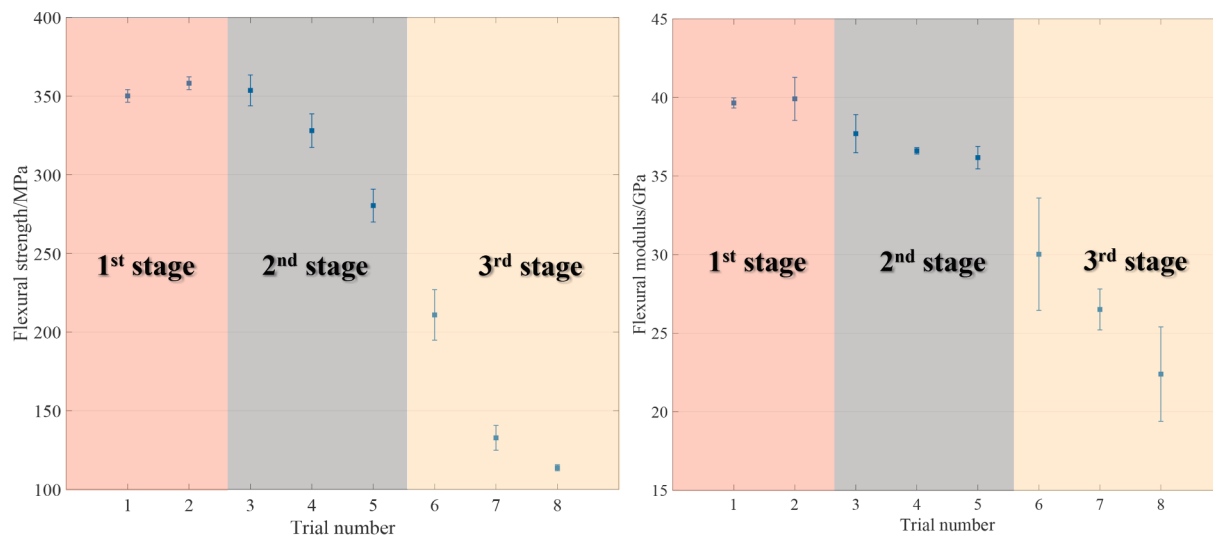


Fig. 4. Front view of stretching simulation schematic diagram of CFRTSTPCs system with different volume fractions taken at a printing temperature of 200°C, printing speed of 600 mm/min.



(a) Experimental results of flexural strength (b) Experimental results of flexural modulus

Fig. 5. Schematic view of the flexural properties conducted CFRTSTPCs.

Firstly, the PET-G polymer simulation box was established in LAMMPS to obtain the material properties. Specifically, the simulations were given out under the NPT ensemble with different printing temperatures (shown in Table 1) and an axial tension was employed with a strain rate of $5 \times 10^{-6} \text{ s}^{-1}$. A series of stress – strain curves from the tensile responses are depicted to calculate Young's modulus and Poisson's ratio. The elastic properties of PET-G are presented in Table 2. Despite the printing temperatures exceeding the T_g (glass transition temperature) of epoxy, the material properties of carbon fibre bundles are assumed to remain constant during the short printing process, spanning temperatures from 210 to 245 °C.

The elastic properties of the carbon fibre bundle are presented in Table 3. Based on the periodic homogenization method, the modified rule of mixtures with stress partitioning parameters [61] was adapted to calculate the constitutive relation of the composites, as shown in Eq. (2). Following that, the composites are defined as elastic, the properties at different temperatures are given and a spatial average of the engineering stress distribution [62,63] was obtained in Eq. (3). Finally, the results of the boundary condition (Table 4) are applied in following interfacial models.

Table 5

Summary of results for stiffness of PET-G/Epoxy-carbon fibre composites systems.

Temperature (°C)	Fibre volume fraction (%)	Elastic modulus from modified rules of mixtures in Eq. (2) (GPa)	Flexural modulus from experiments results of (GPa)	Fibre efficiency η (%)
27	29.1	74.72	39.97	53
	21.3	55.13	26.78	49
	16.8	43.81	22.52	51

3.3. Calculation of the interaction energy

The interfacial bonding energy represents the non-bonded interaction energy between two molecular groups. The interfacial bonding energy describes the interfacial bonding strength and high energy values indicated strong interfacial adsorption [64,65]. The interfacial bonding energies between different components were used to evaluate the failure pattern of CFRTSTPCs. As mentioned in the previous section, different

$$\left\{ \begin{array}{l} E_{11} = V_f E_{11}^f + V_m E^m, \nu_{12} = V_f \nu_{11}^f + V_m \nu^m, E_{22} = \frac{4\eta_{22} G_{23}}{\eta_{22} + m G_{23}}, \frac{1}{G_{12}} = \frac{1}{V_f + \eta_{12} V_m} \left(\frac{V_f}{G_{12}^f} + \frac{V_m \eta_{12}}{G^m} \right) \\ m = 1 + \frac{4\eta_{22} \nu_{12}^2}{E_{11}}, \frac{1}{\eta_{22}} = \frac{1}{V_f + \eta_k V_m} \left(\frac{V_f}{\Lambda_{22}^f} + \frac{V_m \eta_k}{\Lambda^m} \right), \eta_{12} = \frac{1}{2} \left(1 + \frac{G^m}{G_{12}^f} \right), \Lambda_{22}^f = 0.5(K_{22}^f + K_{23}^f), \Lambda^m = 0.5(K_{22}^m + K_{23}^m) \\ \frac{1}{G_{23}} = \frac{1}{V_f + \eta_{23} V_m} \left(\frac{V_f}{G_{23}^f} + \frac{V_m \eta_{23}}{G^m} \right), \eta_{23} = \frac{1}{4(1 - \nu^m)} \left(3 - 4\nu^m + \frac{G^m}{G_{23}^f} \right), \eta_k = \frac{1}{2(1 - \nu^m)} \left(1 + \frac{\Lambda^m}{\Lambda_{22}^f} \right) \end{array} \right. \quad (2)$$

$$\sigma = \frac{\sigma_y^V A}{A_o} \quad (3)$$

pressures and temperatures based on the experimental data listed in Table 1 were applied to the carbon-epoxy and PET-G-epoxy systems. During the simulation, the energy of one component, such as PET-G, was composed of the intra-energy among the PET-G molecules and the interaction energy between the PET-G atoms and other component atoms. Hence, the interfacial bonding energy [64] could be calculated by taking the total energy of the simulation system minus the energy of

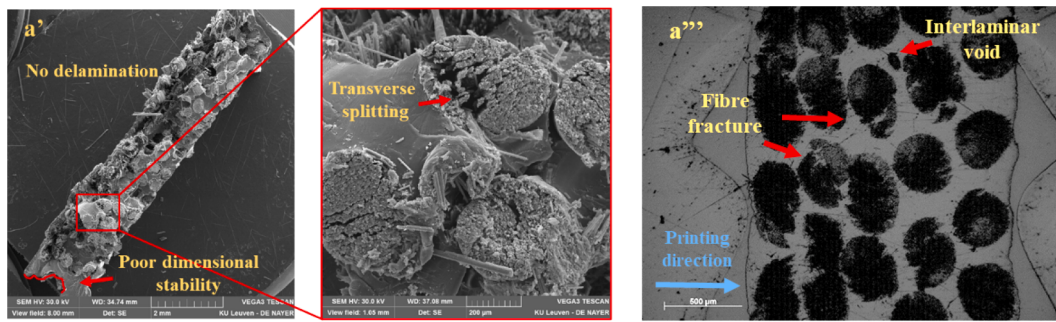
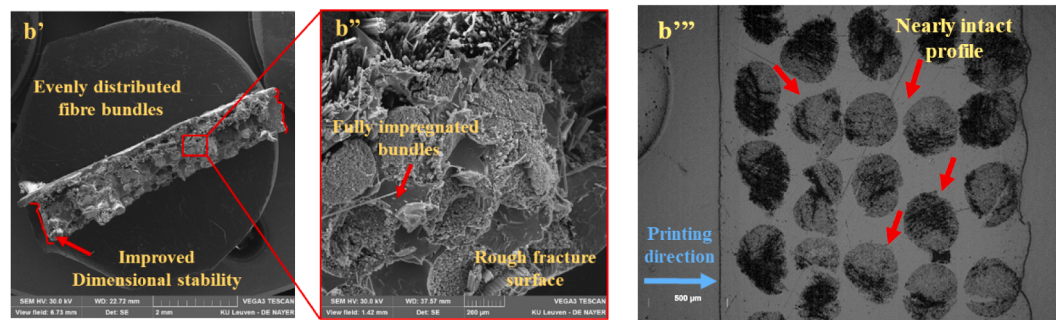
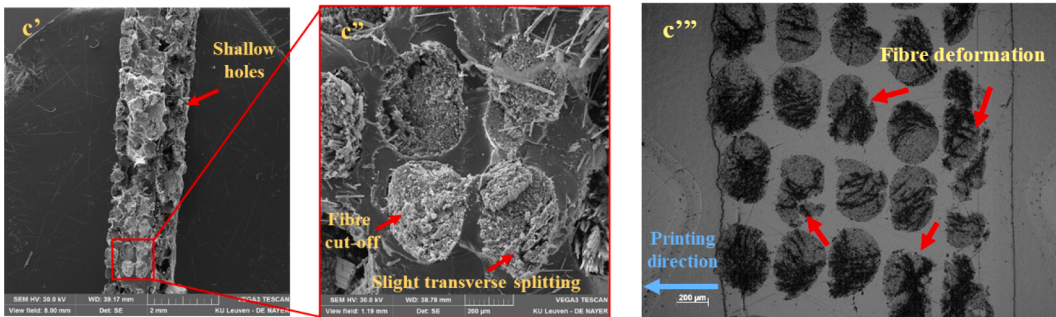
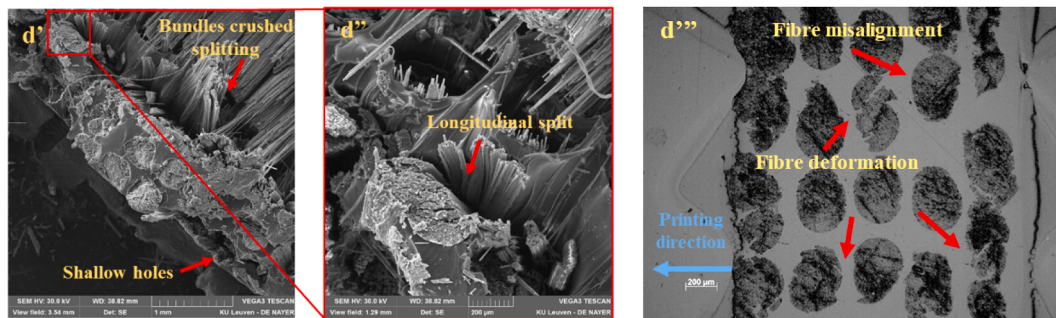
(a) microstructure of CFRTSTPCs with $T = 245\text{ }^{\circ}\text{C}$ (b) microstructure of CFRTSTPCs with $T = 230\text{ }^{\circ}\text{C}$ (c) microstructure of CFRTSTPCs with $T = 215\text{ }^{\circ}\text{C}$ (d) microstructure of CFRTSTPCs with $T = 200\text{ }^{\circ}\text{C}$

Fig. 6. Topographic characterization (including SEM and microscopic images) for different parameters as from Table 1.

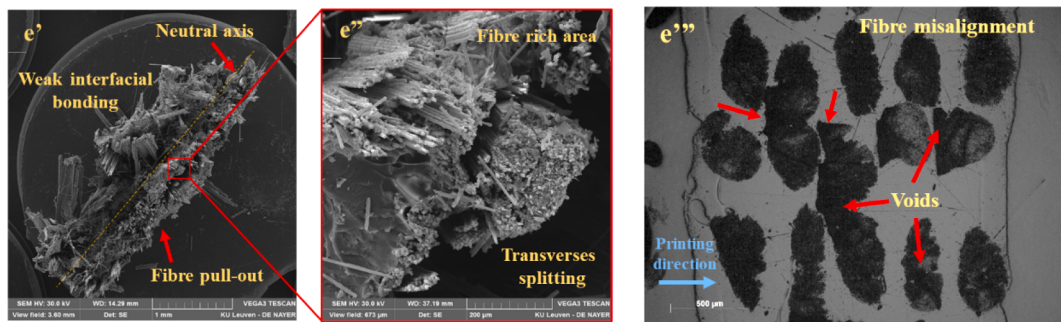
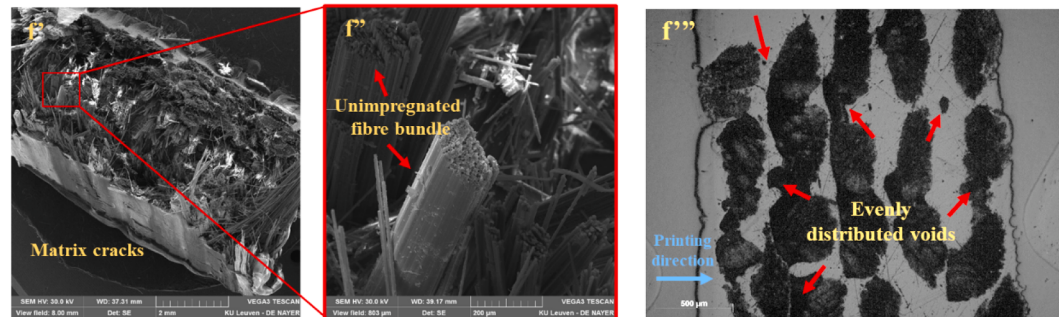
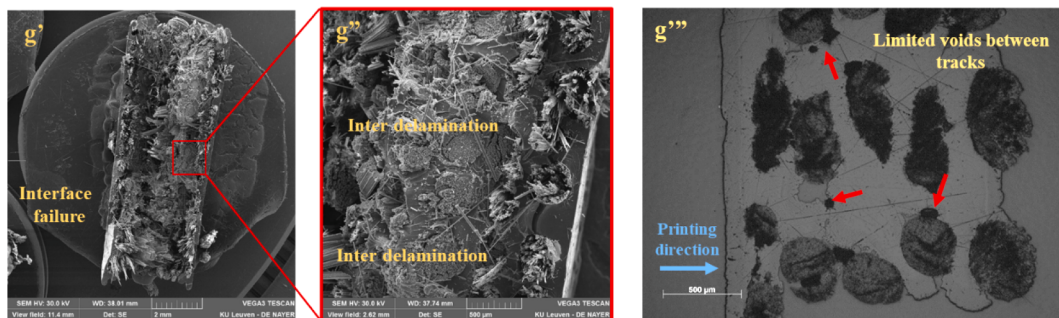
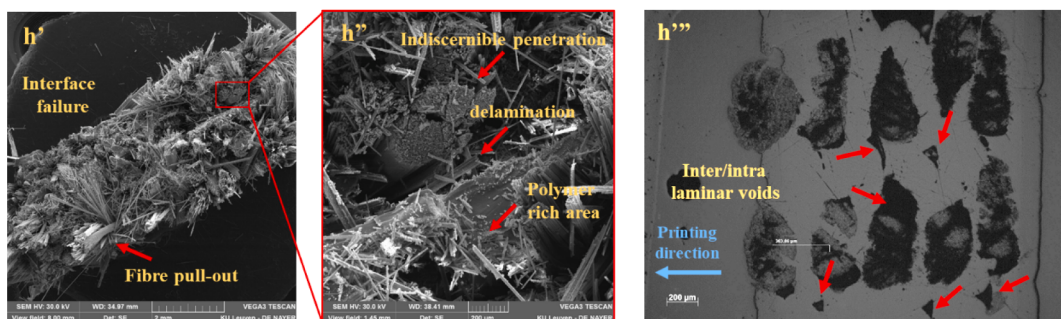
(e) microstructure of CFRTSTPCs with V 300 mm/min (neutral axial)(f) microstructure of CFRTSTPCs with V 600 mm/min(g) microstructure of CFRTSTPCs with H 0.75 mm(h) microstructure of CFRTSTPCs with H 0.95 mm

Fig. 6. (continued).

two components, which could be expressed using Eq. (4):

$$\begin{cases} E_{\text{interface_A}} = E_{\text{Carbon}} + E_{\text{Epoxy}} - E_{\text{Carbon_epoxy}} \\ E_{\text{interface}} = E_{\text{PET-G}} + E_{\text{Epoxy}} - E_{\text{PET-G_epoxy}} \end{cases} \quad (4)$$

where, $E_{\text{interface_A}}$, $E_{\text{interface_B}}$, $E_{\text{Carbon_epoxy}}$, and $E_{\text{PET-G_epoxy}}$ represent the

interfacial bonding energy between carbon fibre and epoxy, interfacial bonding energy between PET-G and epoxy, the total energy of the carbon-epoxy system, and the total energy of the PET-G-epoxy system, respectively; E_{Carbon} , E_{Epoxy} , and $E_{\text{PET-G}}$ represent the energy of carbon fibre, epoxy, and PET-G, respectively.

3.4. Calculation of the elastic moduli

With different value selections of process parameters, the fibre volume fraction of the composite would change which affects the mechanical properties of final printed CFRTSTPCs. To analyse the effect of volume fraction on the mechanical properties, CFRTSTPCs models adopted the same proportions as in the experiments that were built to obtain the axial tensile modulus. As shown in Fig. 2(v), the PET-G, epoxy, and carbon fibre models were placed in a box. Corresponding pressure was applied to the top molecules of PET-G and the bottom of the carbon fibre was fixed. The CFRTSTPCs system was first equilibrated with a NVT ensemble for 1 ns at corresponding temperatures and pressures of Trial 1–8. After that, the system was gradually cooled to room temperature (27 °C) to simulate the actual printing process. Then, the system was equilibrated in an isothermal-isobaric (NPT) ensemble at 27°C and 1 atm for 100 ps to achieve a stress-free state.

Based on the volume fraction of carbon fibre, epoxy, and PET-G in the experiments (shown in Table 1), the PET-G, epoxy, and carbon fibre molecular models were combined in the same proportions by controlling the number of chains. Specifically, the ratio of carbon fibre to epoxy was 3:2 for all the cases, so that the volume fraction of three components could be adjusted just by changing the volume of PET-G and keeping the volume of carbon fibre and epoxy constant. It was observed that the volume of the PET-G model with 20 chains was approximately 2.1 times larger than that of the epoxy model. Therefore, we built PET-G models with 25, 43, and 61 chains to match the volume proportion, as shown in Fig. 4.

To calculate the elastic moduli of these CFRTSTPCs models, a low strain (0.01) in x direction was applied to these models with isothermal-isobaric (NPT) ensemble at 27 °C. The simulation schematic diagram is shown in Fig. 4. To obtain accurate results, the stretching simulation was carried out slowly with a strain rate of $1 \times 10^8 \text{ s}^{-1}$. At a low strain, the stress-strain curves were almost linear and their slopes represented the elastic moduli.

4. Results and discussion

4.1. Flexural strength and modulus of CFRTSTP specimens

After the 3-point bending tests, Fig. 5 presents the experimental results of flexural strength and modulus, including the average values and standard deviations of the 3-point bending tests implemented on the 3D printed samples. In this context, the variation tendency of the flexural properties can be divided into three stages. In the initial stage of Fig. 5

(a), one observes that the flexural strength fluctuates within a certain range. More specifically, starting from a flexural strength of about 350.1 MPa, one observes that the flexural strength slightly increased with a peak of 358.2 MPa (an increase of 2 %) when lowering the temperature from 245 °C to 230 °C. However further increase is not observed when lowering the temperature to 215 °C. In the second stage, the flexural strength is slightly decreased (353.6 MPa to 280.4 MPa, about a 20.7 % drop) with the changes in temperature (from 215 °C to 200 °C) and print speed (from 150 mm/min to 300 mm/min). In the third stage, the flexural strength is significantly decreased (about a 59.5 % drop) when changing print speed and hatch spacing. Ultimately, the minimum reached is 113.7 MPa. Therefore, decreasing the hatch spacing (H), and printing speed (V), while increasing the nozzle temperature (T), will increase the flexural strength [44].

As from Fig. 5(b), the flexural modulus graph follows a similar tendency and the recorded value drops from 39.6 GPa to 22.4 GPa. At the printing temperature of 230 °C, the highest modulus (about 39.9 GPa) is observed. However, the tendency is inapparent when increasing the printing speed from 150 mm/min to 300 mm/min (a moderate drop of about 18.0 % in modulus). From Trial 5 to 8, the flexural strength and modulus dramatically drop when increasing the hatching spacing in the third stage. The reason for the obvious reduction in flexural properties is due to the lower carbon fibre content in CFRTSTPCs. Additionally, defects have a more severe influence on the flexural strength than on the modulus, which could be the primary difference in comparison with the flexural strength graph.

We also compared the experiment results obtained in Fig. 5 and the predicted elastic modulus of Eq. (2) in longitudinal direction are summarised in Table 5. A flexural modulus of 39.97 GPa was used here and this value is the experimental results of trial 2. The last column of Table 1, fibre efficiency η , is calculated by dividing the results of the experiments by the longitudinal elastic modulus of the modified rules of the mixture. A relative alignment between experimental data and theoretical predictions is observed, with the fibre efficiency (η) shifting from 49 % to 53 %, a trend consistent with findings in previous research [66]. This variation can be attributed to factors that cannot be overlooked, such as non-ideal defects in geometric accuracy, porosity content, fibre misalignment, and the interfacial effects present in the specimens. The supposed conditions of modified rules of mixtures are that the interfaces between the components are completely in contact and that the whole composite system is a continuum. At the macroscopic level, only the proportions of each component are taken into account. However, it serves as an intermediary step between experimental observations and molecular dynamics modelling.

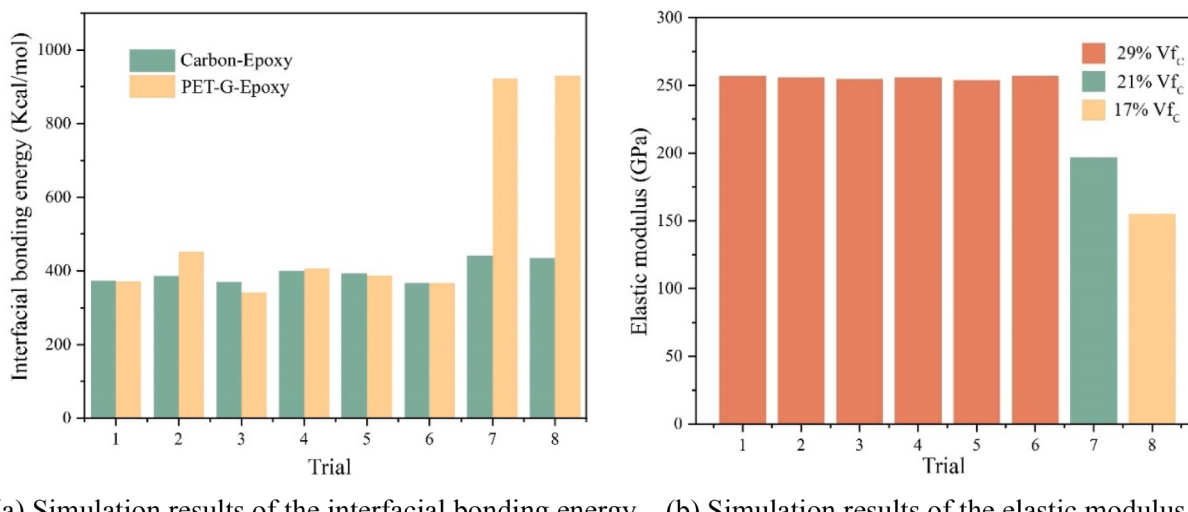


Fig. 7. Results of the molecular dynamics simulation.

4.2. Fractographic behaviour of two-matrix continuous carbon fibre composites

During three-point bending tests, 3D-printed parts endure compression above the neutral layer, and tension below the neutral layer. The SEM and optical images showed that the interfacial bonding performance and defect distribution of CFRTSTPs specimens also changed obviously. Fig. 6(a) to Fig. 6(d) show the fractographic features at the temperatures 245 °C to 200 °C, and at the same time, print speed, hatch spacing, and layer thickness were kept constant. Specifically, a nearly neat fracture section is shown in Fig. 6(a') and the force can be successfully transferred to the fibre bundle, primarily because of strong interfacial adhesion among PET-G, epoxy, and carbon fibre. In addition, a closer observation in Fig. 6(a'') finds that every fibre bundle is fully embedded and connected by PET-G, showing a sufficient embedding of the impregnated fibre bundle. The dimensional stability and surface quality are poor mainly due to the viscosity and flowability of the resin under high printing temperatures. There is also obvious transverse splitting within the fibre bundles, demonstrating the innermost defects, most likely because the bending of the fibre bundle induces shear stresses causing it to split longitudinally, and it becomes easier to produce cracks inside the fibre bundle. From the cross-sectional image of Fig. 6(a'''), similar behaviour of fibre deformation can be noticed, most likely subjected to the manufacturing process.

In Fig. 6(b', b'', b'''), the roundness of fibre bundles is slightly improved in CFRTSTPCs with $T = 230$ °C. As shown in Fig. 6(b'), the micrograph of the fracture surface shows that the fibre bundles and the PET-G are evenly distributed, and some fibre bundles are cut off. In Fig. 6(b''), the fracture shape is comparatively rough, illustrating that distortion and tearing occur and cause irregular surface morphology. This is due to the presence of ductile material, PET-G, that disperses stress, absorbs fracture energy, and generates plastic deformation. During the loading process, the main cracks were deflected several times, so that it hinders the propagation of fracture cracks and a stable failure stage evolved into an unstable fracture stage. These features are beneficial to the performance of CFRTSTPCs and the dimensional stability is also promoted by lowering printing temperature. In Fig. 6(b'''), the profiles of the fibre bundle are nearly intact and no obvious defects occur. Fig. 6(c') shows a more uneven fracture surface with finite fibre pull-out and some shallow holes at 215 °C. In Fig. 6(c''), a more compact failure surface with fibre cut-off along the vertical direction appears suggesting a brittle fracture pattern and fibre bundles are still the primary loading constituent. Slight transverse splitting within the fibre bundles can be observed which is attested by optical microscopy analysis in Fig. 6(c''').

Fig. 6(d') shows a small amount of fibre bundles crushed splitting and pulling out after compressive buckling corresponding to the printing temperature of 200 °C. This shows very poor bonding between the filaments and healing between the printed tracks is incomplete. The corresponding failure regions propagate transversely following the innermost defects of fibre bundles and intra-delamination happens. In Fig. 6(d''), there is a longitudinal splitting inside the composite bundle. As from Fig. 6(d'''), it is also clear that more intra-filament cracks and slight fibre misalignment are generated likely due to increased compaction stress (Table 4). Specifically, the interlayers bonding (between PET-G and PET-G) is governed by the creation of intimate contact and healing, requiring appropriate temperature, time and compaction stress. The temperature influence is through the viscosity and flowability of the matrix. Healing and compaction stress are related to molecular mobility across the contact surface.

In Fig. 6(e'), inter/intra delamination and fibre rupture can be seen in CFRTSTPCs with V300 mm/min illustrating the weak interfacial bonding between layers and debonding failure. Moreover, there is a neutral axis that divided the fracture surface into two parts, where the upper section is subjected to compression and the other layer is subjected to tension. The fact that in the upper section, the fibre pulling-out

is long indicates that the load can be barely transferred to the fibres and interlayer structural damage happens. Fig. 6(e'') provides a more detailed view of the distribution of fibre and matrix. It can be concluded that most fibre bundles are fractured and some fibre-rich/polymer-poor areas are generated, which is in agreement with the observation in Fig. 6(e'''). Compared with Fig. 6(d), a limited melting period and uneven heat might be the reason for the composite deterioration with increasing print speed. Specifically, less heat will be transferred to the composite in the nozzle and the time for applying pressure is shorter.

By comparison, Fig. 6(f), Fig. 6(g) and Fig. 6(h) show CFRTSTPCs microstructures with V600/H0.55, V600/H0.75 and V600/H0.95, respectively. Similar fracture patterns can be observed among these specimens, leading to low flexural properties. Obvious delamination appears indicating the fact that the PET-G matrix cracks first, and the load cannot be transferred to the fibre bundles. Hence, under the mentioned processing parameters, the interfacial bonding between adjacent layers is poor, hence, the failure pattern of the printed sample is interface failure, the matrix crack and pulling-out of the fibre. Besides, there are many intra-/inter-laminar voids (within and along the printing tracks) resulting in the lack of contact between the printing tracks and rapid propagation of cracks along defects. Whereas, Fig. 6(f') and (f'') show fibre bundles are almost debonded from the matrix and voids mainly exist between adjacent tracks and interlayers. Though fibre bundles are deformed, PET-G is difficult to close the gap at such large hatch spacing and high viscosity. Also, the epoxy resin adhered to the carbon fibre surface showing the strong interface into the composite structures. With a further increase of hatch spacing to 0.75 mm (Fig. 6(g)), voids between adjacent tracks diminished, but interfacial adhesion between the fibre bundle and PET-G is still weak. In Fig. 6(h''), no further improvement can be observed and indiscernible penetration with fibre bundles outside being coated. In Fig. 6(h'''), one observes that interlaminar voids with diamond shapes are more apparent. Thus, the defects are significantly affected by the contact of two adjacent printed tracks in a finite space defined by hatch spacing and layer thickness.

In summary, these three process parameters have collaborative effects on the interfacial performance of 3D-printed CFRTSTPs as shown in the cross-sectional surface of Fig. 6. Affected by bonding performance in two interfaces and the number of defects, the fracture patterns of parts are more complex, which may provide a reference for other multiple matrix materials.

4.3. Molecule dynamics analyses

At the initial stage of the interface-forming process, there is an apparent gap between PET-G and epoxy. As the simulation proceeded, PET-G chains were pushed due to the forming pressure and print temperature. The gap gradually disappears and an interface is formed where the intermolecular permeation of PET-G chains and epoxy chains is observed, resulting in interlocking nanostructures. The mechanical interlock effect of these nanostructures has a positive impact on the interface formation of polymers. The interface formation process between carbon fibre and epoxy is similar to that between PET-G and epoxy, but epoxy atoms adhere to the carbon fibre surface without interlocking. This different form of interface formation is one reason leading to different failures of CFRTSTPCs.

The interfacial bonding energies of PET-G-epoxy and carbon-epoxy at different combinations of process parameters are shown in Fig. 7(a). For the carbon-epoxy system, in the cases of Trials 1–3 as depicted in Fig. 7(a), variable temperature and pressure were applied to the carbon-epoxy system. Under the coupling influence of temperature and pressure, the peak of the interfacial bonding energy is observed for Trial 2 (386.1 Kcal/mol), which is slightly higher than that of Trial 1 (372.6 Kcal/mol) and Trial 3 (370.4 Kcal/mol).

According to the Lennard-Jones potential energy function, as the temperature increases, the thermal vibration and the amplitude of atoms also increase in the interface-forming process. The kinetic energy

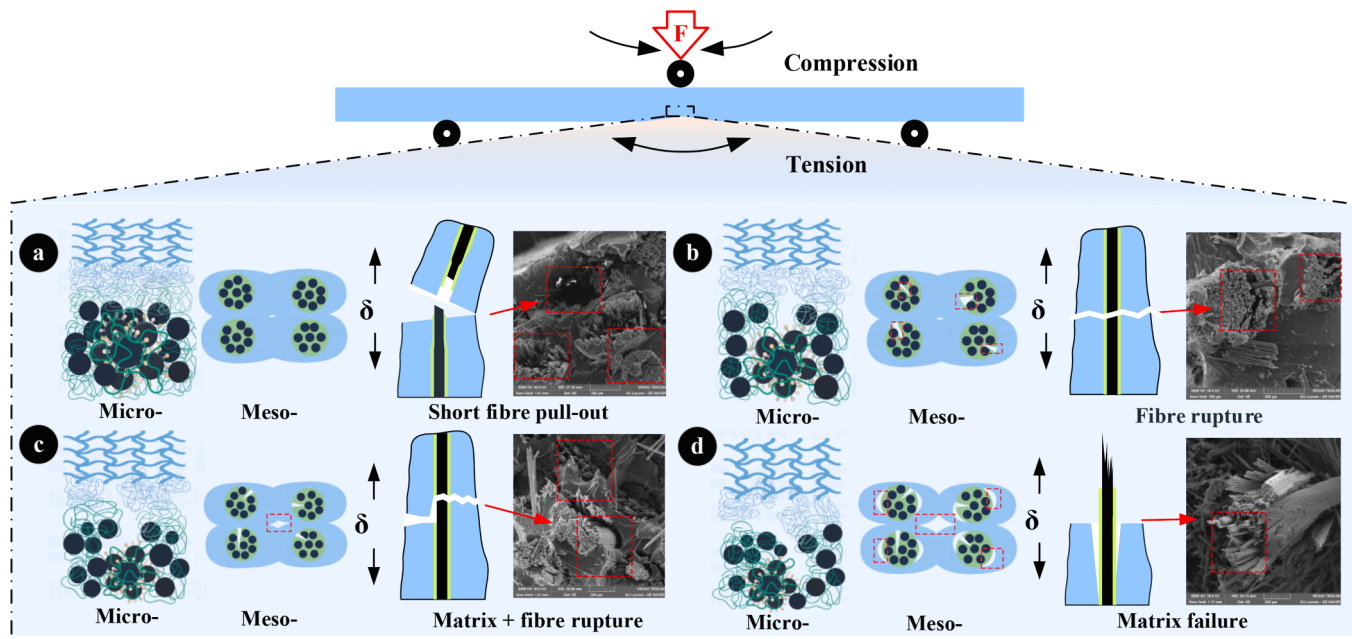


Fig. 8. Fracture patterns and interfacial interactions of 3D printed CFRTPTPCs in multiscale space.

between molecules rises intensifying the thermal motion of atoms and molecules, known as the thermal expansion effect. Therefore, high temperatures can improve interfacial strength by increasing the mobility of polymer chains which promotes the generation of secondary bonds. However, further elevation of temperature leads to an increase in thermal expansion, causing greater atomic fluctuations at the interface and hampering the formation of stable non-bonding forces at the interface. Therefore, excessive temperature will jeopardise the interfacial performance. This trend of interfacial strength variation with elevating temperature is similar to the experimental results. As the printing speed increased, the interfacial bonding energy slightly decreased from 367.79 Kcal/mol (Trial 6) to 441.3 Kcal/mol (Trial 7). Though the epoxy system is a stable structure, the interface interactions are still affected by the printing process. Then the interfacial bonding energy rises when increasing compaction stress. Herein, high pressure can promote interfacial performance because high pressure increases interfacial strength by pushing more epoxy atoms attaching to the carbon fibre surface.

The interfacial bonding energy of the PET-G-epoxy system follows a similar pattern with changes in temperature and pressure as that of the carbon-epoxy system. In the cases of Trials 1–3 as depicted in Fig. 7(a), the peak of the interfacial bonding energy is observed for Trial 2 (452.4 Kcal/mol), which is slightly higher than that of Trial 1 (371.2 Kcal/mol) and Trial 3 (341.5 Kcal/mol). This indicates the effect of temperature on the interfacial bonding and the reason is similar to that of the carbon-epoxy system. Moreover, as shown in the cases of Trials 4–8 in Fig. 7(a), the interfacial bonding energy is influenced by the compaction stress. The difference is at exceptionally high-pressure cases (Trial 7 and 8), the interfacial bonding energy of PET-G-epoxy remarkably increases more than that of carbon-epoxy. Considering the manufacturing process of this typical process and previous research on pre-impregnated fibre bundles [66], the carbon fibres are first impregnated with epoxy and then coated with PET-G in a nozzle of the Anisoprint composer. We do not focus on the impact of resin curing here when printing unidirectional composite material. In that case, the interface bonding between PET-G and epoxy is generated by secondary bonds and mechanical interlocking. Though the epoxy was cured, the molecular chains of PETG are sensitive to high temperatures, and a slight interaction on the interface increases the contact area when PET-G and epoxy interact, causing mechanical interlocking. The compaction stress and temperature are

still significant in reducing the intermolecular distance and the compatibility between layers will be influenced by the process parameters. Besides, the expected deformation of pre impregnated fibre bundles was not observed due to limited simulation scale.

As aforementioned, CFRTSTPC models with different volume fractions were built. The relationship between the proportions of PET-G, Epoxy, and Carbon and the trial setting is shown in Fig. 7(b). Then, a slight strain stretch was applied to these models to calculate the elastic moduli of CFRTSTPCs. The calculated elastic moduli of CFRTSTPCs are shown in Fig. 5. The elastic modulus of Trial 1–6 are roughly 255.0 GPa, the elastic modulus of Trial 7 is roughly 197.0 GPa, and the elastic modulus of Trial 8 is roughly 155.0 GPa. The elastic modulus of Trials 1–6 is essentially the same and this demonstrates that the elastic modulus of CFRTSTPCs is mainly determined by the volume fraction of carbon fibre and is not very dependent on forming temperature and pressure. The values of elastic modulus are higher than the results obtained in Table 5. This discrepancy can be attributed to the simplification of the carbon fibre system as graphene during the modelling process, given that the elastic modulus of graphene falls within the impressive range of 1 TPa. The findings of these MD simulations provide evidence that process parameters affect the interaction and mechanical properties and also an interesting approach for further investigation in CFRTSTPCs.

In summary, it strongly demonstrates that the interfacial performance and volume fraction of carbon fibre can effectively influence the mechanical properties. However, due to the scale limitation of molecular dynamics models, the enhancement effect is not simply correlated, so the process optimisation strategy must be given based on the actual situations when generalising to other multiple matrix composites.

4.4. Multi-scale characteristic of the CFRTSTPCs

As is known for CFRTSTPCs, thermoplastic resins absorb energy, while thermosetting resins provide efficient stress transfer around the carbon fibre [21]. However, these are contingent upon the assumption of ideal interfacial bonding. The actual formation of interfaces is significantly influenced by the manufacturing process. The creation of non-covalent bonds and interactions among various molecular chains can be influenced by the printing process. Owing to these changes, there exist the multiscale chaining effects that initially apply to the micro-

scale until extend to the macro scale in interfacial interaction, thereby affecting the quality of printed components. To the best of our knowledge, there has been no investigation into the multifaceted behaviours of multiple interfaces during their manufacturing process. With this in mind, this study highlights the varied responses in mechanical properties and the interfacial enhancement mechanism influenced by distinct process parameters. It can be found from the above analysis results that the impact of parameters on the flexural property is similar to their effect on interfacial bonding energy. For example, in the first stage (Trial 1 to 3), the effect on the flexural property is consistent with the results of interfacial bonding energy with a peak around 230 °C. This shows that enhanced van der Waals forces, intermolecular forces, and indiscernible defects will be greatly obtained based on the appropriate processing parameters. When increasing print speed from Trial 4 to 6, both interfacial bonding energy and bending performance gradually decrease. In Trials 7 and 8, though the interfacial bonding energies are significantly improved due to the high compaction stress, the fibre volume fraction is the primary factor affecting mechanical performance (fibre volume fraction dropped from 29 % to 17 %). It confirms the fact that increasing the fibre volume fraction within the FFF printing process can achieve higher strength of the two-matrix composites. The main divergence between the simulation and experiments is attributed to the macro-defects. For example, the bonding energy is relatively large in Trial 3, whereas, the bending performance is poor. The morphology analysis revealed that, during the printing process, a significant number of defects are formed due to the compression-induced fracture of fibre bundles. As a result, the observed enhancement in interfacial bonding energy in localized regions does not have a significant impact on the bending performance of printed samples, and a degradation of mechanical performance is envisaged.

Through a comparative analysis of simulation and experimental testing, it becomes evident that the interface between each component plays a pivotal role. During the printing process, the geometric shape and printing trajectory of the parts significantly influence the thermal history and stress distribution, consequently affecting the bonding quality. Thus, connecting the impact on macroscopic and microscopic structural behaviour provides a viable analytical method. Assurance of a specific process conditions through the printing strategy enables the prediction of structural component quality. Moreover, it is observed that the improvement in mechanical properties cannot be only achieved by increasing local interface bonding energy, especially when defects and fibre volume fraction are not considered. This limitation arises from the focus of molecular dynamics simulations on microscopic interactions among different components. The quantity of macroscopic defects and the degree of interlayer bonding are key factors that also influence mechanical properties.

4.5. Fracture mechanism of CFRTSTPCs

Compared with the composite with single-matrix, the bonding degree of multiple interfaces and fibre content can be considered responsible for the mechanical performance and fracture patterns, which are fundamentally influenced by material properties, temperature and compaction stress [67,68]. Therefore, the interfacial analysis under the printing process provides useful information on the delamination and fracture mechanism in CFRTSTPCs. Taken together, interfacial interactions across multiple scales and fracture patterns are shown in Fig. 8.

When layers of deposited materials adhere to each other with less defects on the mesoscale, as illustrated in Fig. 8a, the effect of interfacial bonding energy is further strengthened. For instance, at T230 °C, the damage process becomes progressive, with varying amounts of energy release causing a specific degree of crack deflection. In this scenario, short fibre pull-out occurs to impede crack propagation, resulting in improved properties. When fibre bundles are slightly deformed, for example under T245 and T215, increasing interfacial bonding energy is

detrimental to the mechanical performance, like brittle materials. Herein, the damage initiation in CFRTSTPCs initiated with carbon fibre rupture when conducting 3-point bending experiments, as illustrated in Fig. 8b. This will lead to rapid catastrophic failure. When the number and size of defects along the printing tracks rise, for example, under T200 and V300, the secondary bonds between molecular chains are formed to achieve strong interfacial bonding energy due to high compaction stress. Considering the number and size of defects and interfacial bonding degree, matrix and fibre rupture will occur simultaneously, as shown in Fig. 8c. When a large number of defects are generated during the printing process, for example, under V600, H0.75, and H0.95, fibre bundles are deformed first and many intra-/interlaminar voids occur within/along the printing tracks. The high interfacial bonding energy between PET-G and epoxy is not expected to play a decisive role. The failure pattern is matrix failure, leading to violent fibre pull-out (see Fig. 8d). The fracture mechanism obtained may be valid for other composites with multiple matrices, and geometries, but need to be verified by further works to achieve the desired performance.

Based on the discussion, it can be concluded that defects and appropriate interfacial bonding energy are the prerequisites to ensure mechanical performance. The defects mainly refer to the internal damage of the fibre bundles and the gap between layers and printing tracks. Defects will result in stress concentration and influence crack propagation. Therefore, it is possible to obtain full embedding while avoiding resin failure for two matrix continuous carbon fibre composites at proper processing parameters. Combined with the above changes in multi-scale, it is suggested to promote the interlaminar bonding energy and increase fibre volume fraction on the premise of avoiding manufacturing defects, literally, no fibre bundles damaged, and gaps between layers and printing tracks. Moreover, the molecular dynamics simulation is subject to microcosmic level and defects are also indispensable for the mechanical performance. Other future research consists of a comparison of mesoscopic modelling under different printing processes, to clarify the interlayer compatibility and evolution of defects on the broader perspective.

5. Conclusion

A two-matrix composite material comprising a stiff matrix and a flexible matrix provides the advantages of better coherence and toughness. The potential and mechanism of the material are still a limited reported territory, where low-cost composite parts with excellent mechanical potential will replace traditional materials across the industrial field in the near future. In the paper, the multiscale characteristics of the two-matrix continuous carbon fibre have been fully investigated by using FFF. The results attested to the feasibility of manufacturing CFRTSTPCs by the FFF technique. The effect of the processing parameters (temperature, print speed and hatch spacing) on flexural properties, interfacial interaction and fracture modes are explored by using 3-point bending tests, topography analysis, and molecular dynamics simulation. It is feasible to associate the influence on the macro- and microstructural behaviour and propose an optimisation strategy through multi-scale exploration in such a composite part with multiple matrixes. On the basis of the research, the following conclusions are drawn.

- Multi-scale coupling analysis is an effective way to capture the macroscopic and microscopic damage behaviour. Using this methodology, the failure mechanism can be attributed to the interaction between microscale structure and macroscopic characteristics: increased temperature and compaction stress properly can lead to a higher interfacial bonding energy and consequently enhance the mechanical properties. Nevertheless, the macroscopic features such as fibre bundle deformation, misalignment, and porosity content will jeopardize the interfacial bonding as well.
- The fracture mode of two-matrix continuous carbon fibre composite materials is more complex than that of traditional single resin

composites. There is only van der Waals force between carbon fibres and matrix. However, if the technological processing parameters can be improved, the bonding force is easily generated between resins due to the molecular chain interaction. As for process optimisation of 3D printed CFRTSTPCs, we should enhance interfacial bonding energy and fibre volume fraction on the premise of avoiding manufacturing defects.

- Similar to fibre sizing, the bonding performance between resins can be effectively improved by using a reasonable range of process parameters in FFF, confirming the rationality of the two-resin combination, and allowing for the design of more composites for variety and synergistic performance improvement. Based on that, this prompts us to seek improved mechanical performance and stable interfacial behaviour in the synergistic effect of matrixes which is a subject of a future study.
- The approaches shared in this research present the first step towards designing a real-time predictive analysis model to achieve the desired performance and geometry after the printing process, which will be discussed in future. Moreover, due to the limitations of molecular dynamics methods, it is challenging to analyse the interlayer interfaces between identical materials (such as PETG-PETG) during the FFF process. Additionally, the impact of forming process parameters on macroscopic defects cannot be adequately assessed using this approach. Therefore, future research endeavours will leverage computational fluid dynamics for a more in-depth analysis of the printing process, aiming to gain insights into the influence patterns of these parameters on macroscopic defects.

CRediT authorship contribution statement

Fei Liu: Writing – original draft, Data curation, Conceptualization, Formal analysis, Funding acquisition, investigation, Methodology, Resources, Software, Validation. **Shenru Wang:** Writing – original draft, Conceptualization, Data curation, Formal analysis, Resources, Software, Visualization. **Wuxiang Zhang:** Writing – review & editing, Funding acquisition, Supervision, Project administration. **Xilun Ding:** Writing – review & editing, Project administration, Supervision. **Eleonora Ferraris:** Writing – review & editing, Investigation, Methodology, Supervision. **Jan Ivens:** Conceptualization, Formal analysis, investigation, Methodology, Supervision, Writing – review & editing.

Declaration of competing interest

The authors declare that they have no known competing financial interests or personal relationships that could have appeared to influence the work reported in this paper.

Data availability

Data will be made available on request.

Acknowledgement

This work is supported by National Natural Science Foundation of China (Grant No. 52205003) and Ningbo Key Projects of Science and Technology Innovation 2025 Plan (2022Z070). The authors would like to acknowledge Loren De Vogelaer, Prof. Xin Yan and Junfan Shang for their technical support.

References

- [1] Staszewski WJ, Mahzan S, Traynor R. Health monitoring of aerospace composite structures—Active and passive approach. *Compos Sci Technol* 2009;69:1678–85.
- [2] Li N, Li Y, Jelonmek J, Link GGJ. A new process control method for microwave curing of carbon fibre reinforced composites in aerospace applications. *Compos Part B Eng* 2017.
- [3] Rauh S, Kolb M, Geistbeck M, Boujenfa S, Suess M, Dilger KBK. UV-laser cleaning and surface characterization of an aerospace carbon fibre reinforced polymer. *Int J Adhes Adhes* 2018;82.
- [4] Sujit D. Life cycle assessment of carbon fiber-reinforced polymer composites. Springer; 2011.
- [5] Friedrich K, Almajid AA. Manufacturing Aspects of Advanced Polymer Composites for Automotive Applications. *Appl Compos Mater* 2013.
- [6] Yu L, Zhu C, Sun XH, Salter J, Long R. Rapid Fabrication of Malleable Fiber Reinforced Composites with Vitrimer Powder. *ACS Appl Polym Mater* 2019;1.
- [7] Keller T, Riebel F, Valley T. GFRP posts for railway noise barriers - Experimental validation of load-carrying performance and durability. *Compos Struct* 2008;85: .116-125.
- [8] An A, Mr B. Investigating the feasibility of a new testing method for GFRP/polymer foam sandwich composites used in railway passenger vehicles. *Compos Struct* 2020;233:1–15.
- [9] Garrido M, Correia JR, Keller T, Branco FA. Adhesively bonded connections between composite sandwich floor panels for building rehabilitation. *Compos Struct* 2015;134:255–68.
- [10] Gade P, Gade HS, Gade N. A novel technique for intraradicular rehabilitation using MTA, fiber post and composite: A case report 2016.
- [11] Demertzis M, Silvestre JD, Duro V. Life cycle assessment of the production of composite sandwich panels for structural floor's rehabilitation. *Eng Struct* 2020; 221:111060.
- [12] Akay M, Aslan N. Numerical and experimental stress analysis of a polymeric composite hip joint prosthesis. *J Biomed Mater Res* 1996;31:167–82.
- [13] Chae YJ, Gong HS. Revision Total Elbow Replacement Arthroplasty with an Allograft-Prosthesis Composite: Case Series and Technical Points. *Arch Hand Microsurg* 2020;25.
- [14] Feng C, Cen J, Wu T, Hou T, Chen K, Li X ZD. Preparation and Properties of the Poly(ether ether ketone) (PEEK)/Nano-Zinc Oxide (ZnO)–Short Carbon Fiber (SCF) Artificial Joint Composites 2022.
- [15] Liu H, Falzon BG, Dear JP. An experimental and numerical study on the crush behaviour of hybrid unidirectional/woven carbon-fibre reinforced composite laminates. *Int J Mech Sci* 2019.
- [16] Song L, Meng S, Xu C, Fang G, Xie W. Crack kinking and tunneling simulation for the single-fiber composite under transverse tension based on phase-field method. *J Strain Anal Eng Des* 2020;55:145–58.
- [17] Ge J, Qi L, Chao X, Xue Y, Li H. The effects of interphase parameters on transverse elastic properties of Carbon-Carbon composites based on FE model. *Compos Struct* 2021;268:113961.
- [18] Saeed K, McIlhagger A, Harkin-Jones E, McGarrigle C, Dixon D, Shar MA, et al. Characterization of continuous carbon fibre reinforced 3D printed polymer composites with varying fibre volume fractions. *Compos Struct* 2022;282:115033.
- [19] Vasil'ev VV, Salov VA. Development and examination of a two-matrix glassfiber composite with high transverse strain. *Mech Compos Mater* 1985;20:463–7.
- [20] Azarov AV, Antonov FK, Vasil'ev VV, Golubev MV, Krasovskii DS, Razin AF, et al. Development of a two-matrix composite material fabricated by 3D printing. *Polym Sci Ser D* 2017;10:87–90.
- [21] Callens SJP, Bergsma OK. Two-matrix composites: Carbon fiber micropultrusions embedded in flexible epoxy matrices. *Compos Part A Appl Sci Manuf* 2018;114: 1–12.
- [22] Adumitroaie A, Antonov F, Khaziev A, Azarov A, Golubev M, Vasiliev VV. Novel Continuous Fiber Bi-Matrix Composite 3-D Printing Technology. *Materials (Basel)* 2019;12:3011.
- [23] Yang C, Tian X, Liu T, Cao Y, Li D. 3D printing for continuous fiber reinforced thermoplastic composites: mechanism and performance. *Rapid Prototyp J* 2017.
- [24] Hocheng H, Puw HY. On drilling characteristics of fiber-reinforced thermoset and thermoplastics. *Int J Mach Tools Manuf* 1992;32:583–92.
- [25] He Q, Wang H, Fu K, Ye L. 3D printed continuous CF/PA6 composites: Effect of microscopic voids on mechanical performance. *Compos Sci Technol* 2020;191:1–9.
- [26] Zhuo P, Li S, Ashcroft IA, Jones IA. Continuous fibre composite 3D printing with pultruded carbon/PA6 commingled fibres: Processing and mechanical properties. *Compos Sci Technol* 2022;221.
- [27] Wang Y, Kong D, Zhang Q, Li W, Liu J. Process parameters and mechanical properties of continuous glass fiber reinforced composites-polylactic acid by fused deposition modeling. *J Reinf Plast Compos* 2021;40:2122–35.
- [28] Makeforged Company US n.d. <http://makeforged.com/>.
- [29] Fayazbakhsh K, Movahedi M, Kalman J. The impact of defects on tensile properties of 3D printed parts manufactured by fused filament fabrication. *Mater Today Commun* 2019;18:140–8.
- [30] Balani SB, Chabert F, Nassiet V, Cantarel A. Influence of printing parameters on the stability of deposited beads in fused filament fabrication of poly(lactic) acid. *Addit Manuf* 2019;25:112–21.
- [31] Mutiyala RS, Park K, Güney EE, Kim G, Lau S, Jackman J, et al. Effect of FFF process parameters on mechanical strength of CFR-PEEK outputs. *Int J Interact Des Manuf* 2022;16:1385–96.
- [32] Zhang Z, Shi J, Yu T, Santomauro A, Gordon A, Gou J, et al. Predicting flexural strength of additively manufactured continuous carbon fiber-reinforced polymer composites with machine learning. *J Comput Inf Sci Eng* 2020;1:1–32.
- [33] Chohan JS, Mittal N, Kumar R, Singh S, Sharma S, Dwivedi SP, et al. Optimization of FFF process parameters by naked mole-rat algorithm with enhanced exploration and exploitation capabilities. *Polymers (Basel)* 2021;13:1702.
- [34] Galos J, Hu Y, Ravindran AR, Ladani RB, Mouritz AP. Electrical properties of 3D printed continuous carbon fibre composites made using the FDM process. *Compos Part A Appl Sci Manuf* 2021;151:106661.

- [35] Khalid MZ, Friis J, Ninive PH, Marthinsen K, Ringdalén IG, Strandlie A. First-principles study of tensile and shear strength of an Fe2Al5//Fe interface. *Comput Mater Sci* 2021;192:1–11.
- [36] Sachdeva G, Lobato A, Pandey R, Odegard GM. Mechanical response of polymer epoxy/BMI composites with graphene and a boron nitride monolayer from first principles. *ACS Appl Polym Mater* 2021;3:1052–9.
- [37] Han Y, Elliott J. Molecular dynamics simulations of the elastic properties of polymer/carbon nanotube composites. *Comput Mater Sci* 2007;39:315–23.
- [38] Yan Y, Xu J, Zhu H, Xu Y, Yang C. Molecular dynamics simulation of the interface properties of continuous carbon fiber/ polyimide composites. *Appl Surf Sci* 2021;563:150370.
- [39] Yin C, Zhao X, Zhu J, Hu H, Song M, Wu S. Experimental and molecular dynamics simulation study on the damping mechanism of C5 petroleum resin/chlorinated butyl rubber composites. *J Mater Sci* 2019;54:3960–74.
- [40] Takari A, Ghasemi AR, Hamadanian M, Sarafrazi M, Najafidoust A. Molecular dynamics simulation and thermo-mechanical characterization for optimization of three-phase epoxy/TiO₂/SiO₂ nano-composites. *Polym Test* 2021;93:106890.
- [41] Shokrieh MM, Rafiee R. Prediction of Young's modulus of graphene sheets and carbon nanotubes using nanoscale continuum mechanics approach. *Mater Des* 2010;31:790–5.
- [42] Roudbari MA, Jorshari TD, Lü C, Ansari R, Kouzani AZ, Amabili M. A review of size-dependent continuum mechanics models for micro-and nano-structures. *Thin-Walled Struct* 2022;170:108562.
- [43] Liu YJ, Chen XL. Evaluations of the effective material properties of carbon nanotube-based composites using a nanoscale representative volume element. *Mech Mater* 2003;35:69–81.
- [44] Liu F, Ferraris E, Ivens J. Mechanical investigation and microstructure performance of a two-matrix continuous carbon fibre composite fabricated by 3D printing. *J Manuf Process* 2022;79.
- [45] Heidari-Rarani M, Rafiee-Afarani M, Zahedi AM. Mechanical characterization of FDM 3D printing of continuous carbon fiber reinforced PLA composites. *Compos Part B Eng* 2019;175:107147.
- [46] International A. Standard test methods for flexural properties of unreinforced and reinforced plastics and electrical insulating materials. ASTM International; 2010.
- [47] Plimpton S. Fast parallel algorithms for short-range molecular dynamics. *J Comput Phys* 1995;117:1–19.
- [48] Stukowski A. Visualization and analysis of atomistic simulation data with OVITO—the Open Visualization Tool. *Model Simul Mater Sci Eng* 2009;18:15012.
- [49] Park S-J. Carbon fibers, vol. 210. Springer; 2015.
- [50] Varshney V, Roy AK, Baur JW. Modeling the role of bulk and surface characteristics of carbon fiber on thermal conductance across the carbon-fiber/matrix interface. *ACS Appl Mater Interfaces* 2015;7:26674–83.
- [51] Wang H, Jin K, Wang C, Guo X, Chen Z, Tao J. Effect of fiber surface functionalization on shear behavior at carbon fiber/epoxy interface through molecular dynamics analysis. *Compos Part A Appl Sci Manuf* 2019;126:105611.
- [52] Li H, Zhang H, Cheng X. The effect of temperature, defect and strain rate on the mechanical property of multi-layer graphene: Coarse-grained molecular dynamics study. *Phys E Low-Dimensional Syst Nanostructures* 2017;85:97–102.
- [53] Yang G, Li L, Lee WB, Ng MC. Structure of graphene and its disorders: a review. *Sci Technol Adv Mater* 2018;19:613–48.
- [54] Stuart SJ, Tutein AB, Harrison JA. A reactive potential for hydrocarbons with intermolecular interactions. *J Chem Phys* 2000;112:6472–86.
- [55] Guha RD, Idolor O, Grace L. An atomistic simulation study investigating the effect of varying network structure and polarity in a moisture contaminated epoxy network. *Comput Mater Sci* 2020;179:109683.
- [56] Gavrielides A, Duguet T, Aufray M, Lacaze-Dufaure C. Model of the DGEBA-EDA Epoxy Polymer: Experiments and Simulation Using Classical Molecular Dynamics. *Int J Polym Sci*; 2019. p. 2019.
- [57] Sun H, Mumby SJ, Maple JR, Hagler AT. An ab initio CFF93 all-atom force field for polycarbonates. *J Am Chem Soc* 1994;116:2978–87.
- [58] Moon J, Yang S, Cho M. Interfacial strengthening between graphene and polymer through Stone-Thrower-Wales defects: Ab initio and molecular dynamics simulations. *Carbon N Y* 2017;118:66–77.
- [59] Koloor SSR, Rahimian-Koloor SM, Karimzadeh A, Hamdi M, Petru M, Tamin MN. Nano-level damage characterization of graphene/polymer cohesive interface under tensile separation. *Polymers (Basel)* 2019;11:14–35.
- [60] Feng T, Rai A, Hun D, Shrestha SS. Molecular dynamics simulations of energy accommodation between gases and polymers for ultra-low thermal conductivity insulation. *Int J Heat Mass Transf* 2021;164:1–10.
- [61] Tsai SW, Hahn HT. Introduction to Composite Materials. *Introduction to Composite Materials* 2018.
- [62] Lyngdoh GA, Das S. Elucidating the interfacial bonding behavior of over-molded hybrid fiber reinforced polymer composites: experiment and multiscale numerical simulation. *ACS Appl Mater Interfaces* 2022;14:43666–80.
- [63] Zhou M, Xiong X, Drummer D, Jiang B. Molecular Dynamics Simulation on the Effect of Bonding Pressure on Thermal Bonding of Polymer Microfluidic Chip. *Polymers (Basel)* 2019;11.
- [64] Wang XQ, Jian W, Buyukozturk O, Leung CKY, Lau D. Degradation of epoxy/glass interface in hydrothermal environment: An atomistic investigation. *Compos Part B Eng* 2021;206:1–11.
- [65] Zhang M, Jiang B, Chen C, Drummer D, Zhai Z. The effect of temperature and strain rate on the interfacial behavior of glass fiber reinforced polypropylene composites: a molecular dynamics study. *Polymers (Basel)* 2019;11:1–18.
- [66] Liu F, Ferraris E, Ivens J. Mechanical investigation and microstructure performance of a two-matrix continuous carbon fibre composite fabricated by 3D printing. *J Manuf Process* 2022;79:383–93.
- [67] Liu T, Tian X, Zhang M, Abliz D, Li D, Ziegmann G. Interfacial performance and fracture patterns of 3D printed continuous carbon fiber with sizing reinforced PA6 composites. *Compos Part A Appl Sci Manuf* 2018;114:368–76.
- [68] Vatanç BB, Uşun A, Yıldız N, Şimşek C, Cora ÖN, Aslan M, et al. Additive Manufacturing of PEEK-Based Continuous Fiber Reinforced Thermoplastic Composites with High Mechanical Properties. *Compos Part A Appl Sci Manuf* 2023; 1074–84.